Target residues from the interaction of copper with 90 MeV/nucleon ^{6}Li ions

J. P. Whitfield and N. T. Porile
Department of Chemistry, Purdue University, West Lafayette, Indiana 47907
(Received 16 July 1993)

Target residues from the interaction of copper with 90 MeV/nucleon ^{6}Li ions have been studied utilizing thick-target, thick-catcher recoil range techniques. Cross sections, average forward ranges, and forward-to-backward ratios have been measured. Isobaric and mass yield distributions have been constructed from the cross section data. Longitudinal momentum transfer information has been obtained. Comparisons with a variety of lighter and heavier projectiles interacting with copper have been made. Comparisons of the data with initial interaction-evaporation models ISABELLE-EVA, BUU-GEMINI, and BUU-PACE are presented.

PACS number(s): 27.70.Mn

I. INTRODUCTION

For many years interactions between light projectiles, $Z \leq 2$, and medium mass targets have been investigated at intermediate energies [1–7]. More recently, experimental results based on the use of heavy ions as projectiles on medium mass targets have been reported [8–16]. Some very interesting phenomena have been shown to occur for beam energies between 10 and 100 MeV/nucleon. As beam energies increase above 10 MeV/nucleon complete fusion gives way to incomplete fusion, which becomes increasingly important with increasing energy. This trend is believed to be a consequence of the diminishing importance of mean field interactions and the increasing importance of two body nucleon-nucleon interactions as energies increase towards 100 MeV/nucleon. By obtaining the linear momentum transferred (LMT) from projectile to target in the initial stage of the interaction one can obtain information about the global features of nucleus-nucleus reactions. It has been shown that for projectiles of $Z > 1$ LMT seems to saturate at $\sim 170 - 220$ MeV/c per incident nucleon for both medium mass and heavier targets [5,6,8,11,17–24]. It has also been shown that lighter projectiles appear to be more efficient than heavier projectiles in transferring momentum on a per nucleon basis [8,11,20,25].

Most of the information reported for medium mass targets has been obtained using thick-target, thick-catcher recoil range techniques, which can be used to measure cross sections and average kinematic properties of individual radioactive nuclides produced in the interaction. Here we employ these methods to study the interaction at 90 MeV/nucleon of ^{nat}Cu with ^{6}Li, which lies between light and heavy bombarding particles. By comparing the results with those for a variety of light-ion and heavy-ion interactions with Cu [1–3,8–13] we investigate the evolution of reaction dynamics with projectile mass into this transitional region. Also, we use various interaction and evaporation models to predict the present reaction residue cross sections and kinematic properties.

II. EXPERIMENTAL PROCEDURE

At the K1200 cyclotron at the National Superconducting Cyclotron Laboratory (NSCL) at Michigan State University, we have utilized a 90 MeV/nucleon ^{6}Li beam of $\sim$54 enA intensity. Intensity measurements were made using a calibrated Faraday cup and recorded using a current integrator. This information was then digitized and recorded at one minute intervals using a multichannel analyzer, so that fluctuations in the beam intensity could be monitored. Details of the experimental setup have been reported previously [8–10]. Briefly, the target stack consisted of a 20.1 mg/cm^2 thick copper foil, surrounded by carbon foils of 10.1 mg/cm^2 thickness, two placed upstream of the target and two placed downstream. The energy of the ^{6}Li beam was reduced to 538 MeV at the center of the target stack due to energy loss in the carbon and copper foils [26,27]. A single irradiation of 8.5 h was performed. The target stack was then returned to Purdue where counting commenced $\sim$7 h after end of bombardment and continued for several months. The individual foils of the stack were counted using calibrated Ge(Li) and intrinsic Ge spectrometers. The code SAMPO [28] was used to determine the intensities of $\sim$80 γ-ray peaks. Decay curves were constructed from these intensities and analyzed using CLSQ [29]. Nuclidic assignments were based on γ-ray energy, half-life and correlation with other γ rays emitted by a presumed nuclide [30].

III. RESULTS

The cross sections of 31 products are listed in Table I. These were determined using techniques described in detail in previous reports from our laboratory [8–10,31]. The uncertainties in the cross sections are the larger of the standard deviation in the mean values of the total set of γ rays for a given product nucleus and the estimated uncertainty of individual determinations of these γ rays. Corrections for fluctuations in beam intensity

have been applied where appropriate. An additional 10% has been folded into the tabulated uncertainties in those cases where only a single γ ray for a particular product was used to calculate the cross section. The values for ^{22}Na, ^{24}Na, and ^{28}Mg were reduced by ~60%, ~30% and ~5%, respectively, due to direct production of these products in the carbon foils. Those products labeled I (independent yields) represent nuclides where no progenitor feed-in is included in the tabulated cross section. Those labeled C^+ include the contribution of proton-rich isobaric progenitors, while the C^- include those of neutron-rich progenitors.

Also listed in Table I are the recoil properties of the given product nuclides, expressed in terms of FW, the average forward range, and F/B, the ratio of forward-to-backward emission. Here, W is the target thickness in mg/cm^2 and F and B are the fractions of total activity of the product nuclide in the forward and backward catchers, respectively. The uncertainties were determined in a similar manner as those in the cross sections. Again, ^{22}Na, ^{24}Na, and ^{28}Mg required substantial reduction in their FW values of ~70%, ~56% and ~16% due to production in the carbon catchers. Eleven other products ranging from ^{43}K to ^{55}Co required reductions by 1 – 3 %. Owing to the low activity observed in the backward catcher, the corrections to B are large, averaging ~70%. The corresponding F/B values have been corrected by factors of ~ 1.5 – 4. These values are listed only to give an indication of their magnitude; they are not used in our subsequent analysis.

TABLE I. Cross sections, forward ranges, and forward/backward ratios for product nuclides from the interaction of copper with 90 MeV/nucleon ^{6}Li ions.

Nuclide	Type	σ (mb)	FW (mg/cm^2)	F/B
^{22}Na	C^+	0.25±0.03	1.95±0.37	
^{24}Na	C^-	0.53±0.06	1.96±0.28	
^{28}Mg	C^-	0.05±0.01	2.21±0.34	
^{42}K	I	2.45±0.27	1.59±0.18	20.7±2.3
^{43}K	C^-	0.87±0.03	1.38±0.06	56.9±5.1
^{43}Sc	C^+	4.24±0.59	0.73±0.14	65.8±34.0
^{44}Sc	I	4.09±0.13	1.02±0.08	18.0±1.4
^{44}Sc^m	I	5.76±0.29	1.24±0.17	64.9±9.1
^{46}Sc	I	7.11±0.06	1.30±0.02	83.9±13.2
^{47}Ca	C^-	0.06±0.03	1.30±0.54	
^{47}Sc	I	2.86±0.31	1.41±0.16	92.9±16.0
^{48}Sc	I	0.65±0.04	1.05±0.06	81.9±8.1
^{48}V	I	12.5±0.1	1.22±0.02	106±10
^{48}Cr	C^+	0.44±0.02	1.05±0.05	116±12
^{51}Cr	C^+	41.1±4.4	1.05±0.11	101±17
^{52}Mn	C^+	14.6±0.2	0.87±0.03	132±16
^{52}Fe	C^+	0.28±0.04	1.05±0.16	
^{54}Mn	I	34.2±3.6	0.89±0.10	69.0±8.9
^{55}Co	C^+	2.43±0.05	0.73±0.04	113±18
^{56}Mn	C^-	5.99±0.01	0.73±0.04	29.4±1.6
^{56}Co	I	13.5±0.4	0.67±0.03	94.6±5.9
^{56}Ni	C^+	0.10±0.01	1.08±0.15	23.1±9.4
^{57}Co	I	47.2±2.4	0.57±0.03	65.7±2.2
^{57}Ni	C^+	1.55±0.07	0.62±0.04	50.4±2.5
^{58}Co	I	51.1±3.9	0.52±0.05	49.3±3.3
^{59}Fe	C^-	2.48±0.04	0.46±0.01	27.2±1.0
^{60}Co	I	14.6±0.6	0.35±0.02	20.0±1.1
^{61}Cu	C^+	27.2±0.9	0.24±0.02	39.4±3.4
^{62}Zn	C^+	1.62±0.07		
^{64}Cu	I	27.9±3.14		
^{65}Zn	C^+	2.06±0.22	0.23±0.01	

IV. DISCUSSION

A. Isobaric yield distribution

We have utilized a modified version of Rudstam's [32] six parameter equation in order to estimate the cross section of those products undetectable by our experimental methods:

$$\sigma(Z,A) = \exp[\alpha_1 + \alpha_2 A + \alpha_3 A^2 + \alpha_4 A^3 + (\alpha_5 + \alpha_6 A + \alpha_7 A^2)|Z_p - Z|^{\alpha_8}], \quad (1)$$

where

$$Z_p = \alpha_9 A + \alpha_{10} A^2. \quad (2)$$

Again, details of the minimization procedure used to obtain the various constant terms in the equation have been previously reported [8–10]. The values obtained for the parameters $\alpha_1 - \alpha_{10}$ are shown in Table II.

Figure 1 shows a comparison of the fractional isobaric yield distribution at A=51 with the data. The data have been scaled by the ratio of the calculated cross section at A=51 and the mass number of the product in question. The results show that the parametrization provides a good fit to the data; the mean deviation of the points from the curve is ~ 20%.

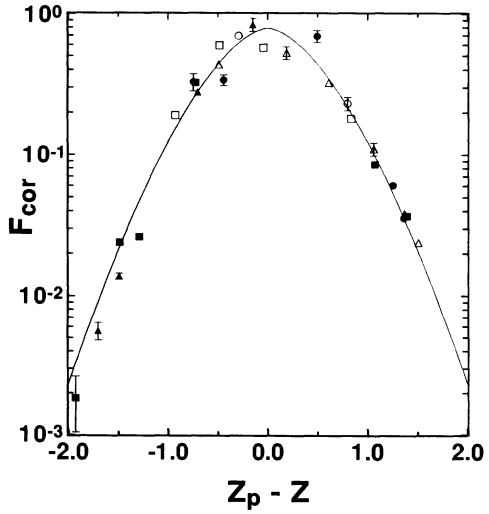

FIG. 1. Fractional isobaric yield distribution for the interaction of copper with 90 MeV/nucleon ^{6}Li ions. The curve represents the fitted values from Eq. (1) and (2) at A = 51; the data are scaled to A = 51. The different symbols indicate the products mass region: (•) A = 22–44, (▲) A = 46–55, (■) A = 56–65. Open symbols represent independent yields.

TABLE II. Parameters employed in the fit of Eqs. (1) and (2) to experimental cross sections from the interaction of copper with 90 MeV/nucleon ^{6}Li ions.

Parameter	Value	Parameter	Value
α_1	5.06±0.87	α_6	$(2.59\pm1.14)\times10^{-2}$
α_2	−0.62±0.07	α_7	$-(4.57\pm1.28)\times10^{-4}$
α_3	$(1.98\pm0.17)\times10^{-2}$	α_8	1.65±0.04
α_4	$-(1.61\pm0.13)\times10^{-4}$	α_9	0.49±0.00
α_5	−1.99±0.25	α_{10}	$-(4.17\pm0.12)\times10^{-4}$

We have compared the present data with those for other projectiles incident on copper targets at comparable energies, including 590 MeV protons [2], 258 MeV ^{3}He [1], 410 and 720 MeV α [3], as well as 527 and 1073 MeV ^{12}C [8,9]. For those reactions where our group was not directly involved with the data analysis we have, for the sake of consistency, utilized the above ten-parameter equation in order to obtain isobaric yields from the reported cross sections. For these seven different reactions we have found that the full width at half maximum (FWHM) and Z_p, the most probable charge at A=51, are constant within the limits of error. The constancy is documented in Fig. 2, which shows the variation of these parameters with total projectile kinetic energy.

B. Mass yield distribution

Experimental mass yield distributions may be obtained by combining the experimental cross sections with those calculated by Eq. (1) at a given mass number A. The results are shown in Fig. 3. A 20% uncertainty in the calculated yields has been included in the overall uncertainty of each total isobaric yield. The curve through the data is the yield obtained solely from Eq. (1). It is seen that the parametrization provides a good fit to the data. The mass-yield curve becomes uncertain above $A \sim 64$ because ^{63}Cu is less likely to contribute to the yields than ^{65}Cu. We have estimated the cross section at $A = 65$ by normalizing the yield predicted by Eq. 1 for ^{65}Zn, the most likely product at this mass number, to the experimental yield.

The mass yield distribution exhibits a broad peak at $A\sim$ 60 and the yields decrease at lower masses, the decrease being exponential over most of the observed mass region. The curve is compared with similar curves obtained for copper plus ^{12}C in Fig. 4(a). Results are shown for 45 MeV/nucleon ^{12}C [10] which has comparable total kinetic energy, and for 90 MeV/nucleon ^{12}C [8], with the same energy per nucleon. Although all the curves have similar overall shape, several significant differences between ^{6}Li and ^{12}C may be noted. Thus, the peak in the ^{6}Li curve is shifted to a larger mass by 3 to 6 mass units. This difference suggests that preequilibrium emission may be more extensive for the heavier projectile. Furthermore, the increase in the yields of the lightest products, $A \leq 30$, observed for ^{12}C is not evident for

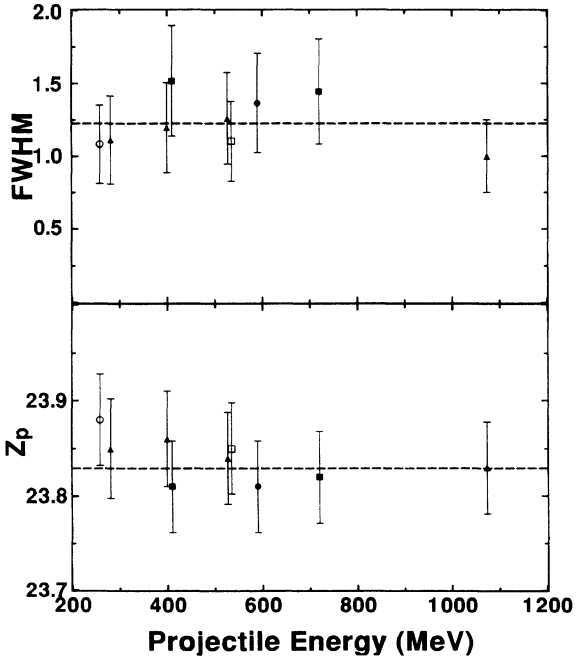

FIG. 2. Projectile energy dependence of (top) the full width at half maximum, and (bottom) Z_p, the most probable charge of the isobaric yield distribution at A = 51. The various symbols indicate the projectile identity: (•) protons [2], (○) ^{3}He [1], (■) α [3], (□) ^{6}Li [present work], (▲) ^{12}C [8,9].

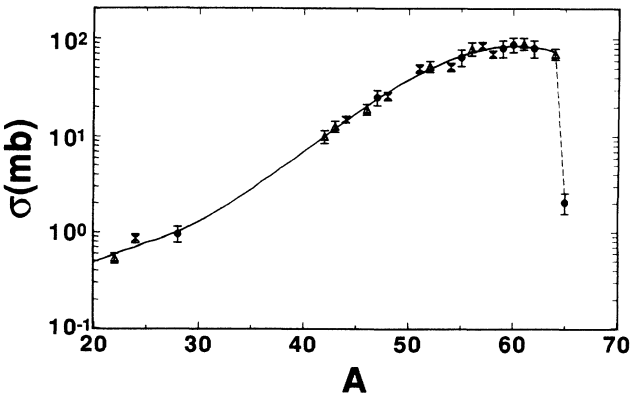

FIG. 3. Mass yield distribution for the interaction of copper with ^{6}Li ions. The solid curve represents the distribution calculated from Eqs. (1) and (2). The points are experimental yields corrected for unmeasured products at a given mass number. The different symbols reflect the fractional contribution of the experimental cross sections to a given isobar: (•) >50%, (△) 20-50%, and (*) <20%. The dashed line is an estimate of the dropoff in yields above A = 64.

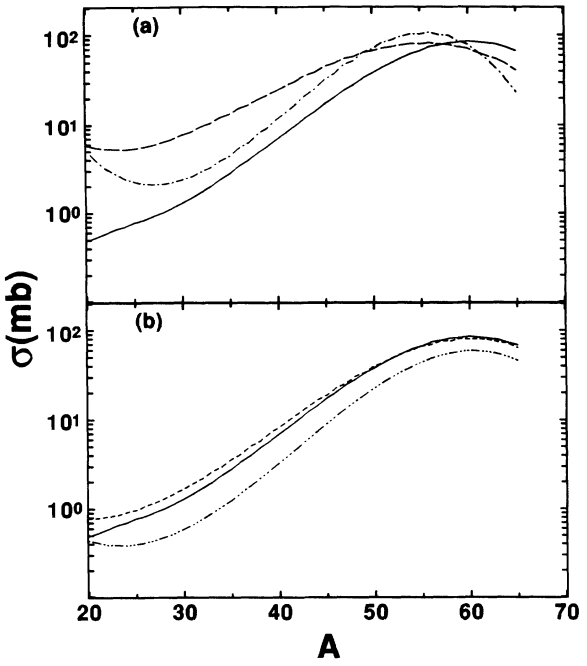

FIG. 4. Mass yield distribution for the interaction of copper with (a) 90 MeV/nucleon ^{6}Li (—), 45 MeV/nucleon (– • –) and 90 MeV/nucleon (- - - - - -) ^{12}C [8,9]; (b) 90 MeV/nucleon ^{6}Li (—), 720 MeV α (- - - - - -) [3], and 590 MeV protons (– • • • –) [2].

^{6}Li, indicating that fragmentation is more important for the heavier projectile.

Figure 4(b) shows a comparison of the ^{6}Li mass yield curve with that obtained for lighter projectiles [2,3]. All three curves have very similar shape, indicating that ^{6}Li is more akin to a light than a heavy ion as far as the shape of the mass yield is concerned. Note that differences in total reaction cross section have not been taken into account so that differences in vertical scale are expected.

Cumming *et al.* [33] have shown that the slope of the exponential region of the mass yield distribution decreases with increasing bombarding energy and eventually becomes independent of energy in the limiting fragmentation regime. Figure 5 shows the slope extracted from a more complete data set [1–3,8–10]. The slope indeed decreases linearly with total kinetic energy for projectiles ranging from protons to ^{12}C ions between 0.2 and 1 GeV. However, it is apparent that the systematic trend in the slopes obscures the very real difference in the mass yield distributions for light and heavy ions depicted in Fig. 4.

C. Linear momentum transfer

A more informative examination of the global features of reaction mechanisms at the energies of present interest can be obtained by analysis of the recoil range data. The velocity along the beam direction of the residual nucleus, $v_{\|}$, and in turn the mean LMT, $\langle P_{\|} \rangle$, can be obtained

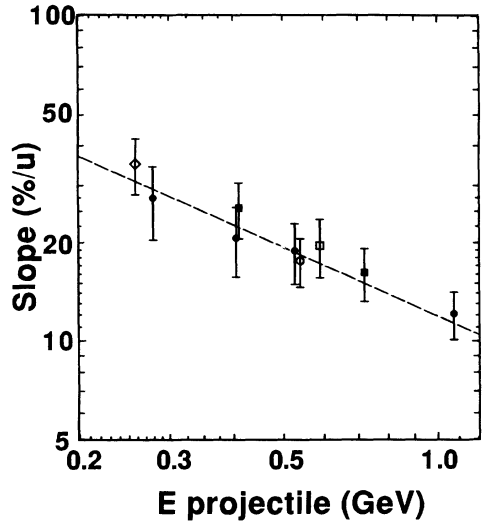

FIG. 5. Comparison of the slope from the exponential region of the mass yield distributions for the interaction of copper with (□) protons [2], (◇) ^{3}He [1], (closed square) α [3], (○) ^{6}Li [present work], (•) ^{12}C [8–10]. The line is a fit to the data.

from the average forward range data FW, as has been discussed previously [8–10]. The present data have been adjusted in accordance with results reported by Whitfield and Porile [34] in order to correct for the overestimation of $v_{\|}$ due to the effect of evaporation on the range-energy conversion. We have utilized the code TRIM [27] to obtain range-energy tables used in this analysis.

The results are shown in Fig. 6 as $v_{\|}/v_{\rm CN}$, the fractional velocity transfer with respect to mass loss from the target, ΔA, where $v_{\rm CN}$ is the velocity of the putative compound nucleus. The values of $v_{\|}/v_{\rm CN}$ exhibit a nearly linear increase with increasing mass loss termi-

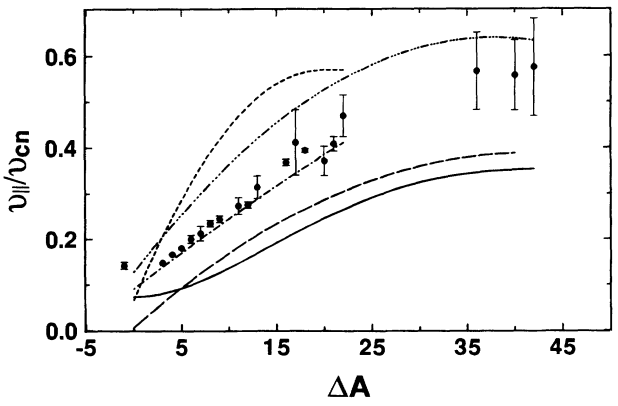

FIG. 6. Fractional velocity transfer for the interaction of copper with 90 MeV/nucleon ^{6}Li ions vs mass loss from the target, ΔA. The various curves show the trends in similar results for the interaction of copper with ^{12}C at 45 (– • • • –) and 90 (—) MeV/nucleon [8,9], and ^{3}He at 86 (– – –), 117 (– •–), and 303 (— —) MeV/nucleon [1].

nating in a leveling off for the lightest products. This trend has a geometrical origin, where near-target products are produced in peripheral interactions while the lightest products are a result of more central collisions [11].

Comparing this fractional velocity distribution with distributions from some of the previously discussed interactions allows us to observe trends in momentum transfer with respect to projectile mass and energy. Figure 6 includes curves showing results for interactions involving copper and 86, 117, and 303 MeV/nucleon ^{3}He [1] as well as 45 and 90 MeV/nucleon ^{12}C [8,9].

The first important trend displayed in Fig. 6 is the decrease in $v_{\|}/v_{\rm CN}$ with increasing projectile velocity. An increase from 86 to 303 MeV/nucleon ^{3}He or from 45 to 90 MeV/nucleon ^{12}C leads to a marked decrease in the fractional velocity transfer over the entire product range. This trend points not only to the increasing dominance of peripheral interactions at higher beam energies [20,21,35] but also to the greater importance of nucleon-nucleon collisions at higher energies and thus to increasing transparency. The second trend involves a change in projectile mass for approximately the same energy per nucleon. Comparing the 86 MeV/nucleon ^{3}He and 90 MeV/nucleon ^{12}C curves with the present data we again see a significant decrease in the fractional velocity transfer with increasing projectile mass. This trend supports previous work showing that lighter projectiles are more efficient in transferring their momentum than heavier projectiles [8,11,20,25]. However, this trend is reversed if the $v_{\|}/v_{\rm CN}$ values are compared for the same projectile kinetic energy. Thus the curve for 45 MeV/nucleon ^{12}C (540 MeV) lies above the values for 90 MeV/nucleon ^{6}Li (540 MeV), while the trend in the ^{3}He curves indicates that ^{3}He at 180 MeV/nucleon should lead to smaller $v_{\|}/v_{\rm CN}$ than ^{6}Li.

The above trends are also evident in a comparison of the mean LMT, $\langle P_{\|}\rangle$. This quantity is obtained by estimating the average mass of the residue leading to a particular product associated with a specific $v_{\|}$. The product of the velocity $v_{\|}$ and the mass of the residue is $P_{\|}$ for the final identified product. By weighting each of these individual $P_{\|}$ by the product formation cross section we obtain $\langle P_{\|}\rangle$. The method used in the estimation of the residual mass has been described elsewhere [8–10]. Figure 7(a) displays the variation in $\langle P_{\|}\rangle/P_{\rm CN}$ with total projectile kinetic energy, where $P_{\rm CN}$ is the momentum of the hypothetical compound nucleus. Results are shown for Cu interacting with 86 – 303 MeV/nucleon ^{3}He [1], 15 – 90 MeV/nucleon ^{12}C [8–10], 17 – 27 MeV/nucleon ^{14}N [11] and 8–48 MeV/nucleon ^{20}Ne [11], along with the present data. As expected there is decreasing fractional momentum transfer with increasing projectile kinetic energy. The results for the heavier projectiles (^{12}C–^{20}Ne) appear to exhibit a linear decrease over the entire energy region of present interest and the values are virtually independent of projectile mass. Similar results have been reported by Leray [24] for central collisions. The lighter projectiles also exhibit a linear decrease, but the slope is smaller and the fractional momentum transfer is not as large. From this analysis ^{6}Li appears to behave more like a light projectile, as was also noted for the mass yield distribution.

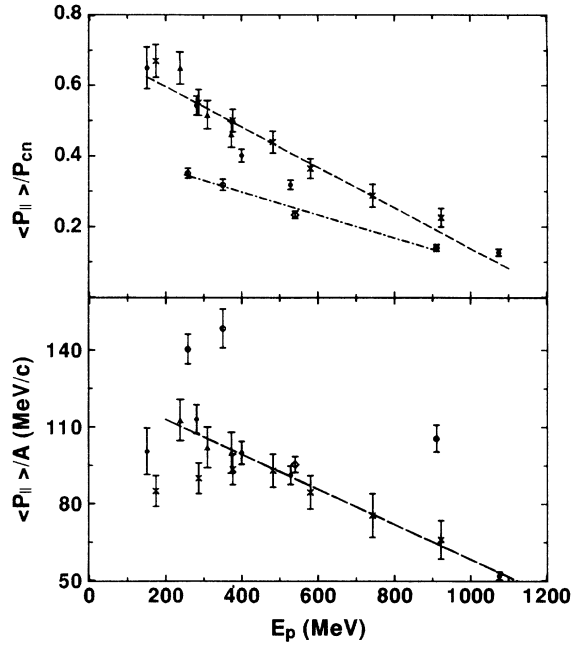

FIG. 7. Projectile energy dependence of (top) the fractional average momentum transfer, and (bottom) the mean linear momentum transfer per incident nucleon. The various symbols indicate the projectile indentity: (○) ^{3}He [1], (◇) ^{6}Li [present work], (•) ^{12}C [8–10], (▲)^{14}N [11] and (*) ^{20}Ne [11]. The lines are linear fits to data.

In Fig. 7(b) the variation of the mean LMT per incident nucleon with total projectile kinetic energy is displayed. Once again the ^{3}He data exhibit results very different from those for the heavier projectiles, yet the ^{6}Li results now appear to be more in line with the heavy ion data. The most interesting result is that for each heavy projectile, independent of mass, above ~25 MeV/nucleon the mean LMT per incident nucleon decreases linearly with increasing projectile energy, suggesting that when heavy ion bombarding energies are increased above the fermi energy the average momentum transferred to the target per incident projectile nucleon scales with total projectile kinetic energy independent of mass.

Figure 6 also shows that with increasing mass loss from the target there is a limitation to the fractional velocity transfer for the lightest products for each of the interactions. This limitation to momentum transfer has been widely documented [5,6,8,11,17–24]. From the values of $v_{\|}/v_{\rm CN}$ in the plateau region we can obtain the maximum momentum transfer $\langle P_{\|}^{\rm max}\rangle$ for each of the interactions. The ^{12}C reactions lead to values of ~170 and ~130 MeV/c per incident nucleon for 45 and 90 MeV/nucleon, respectively. For ^{3}He at 86 and 303 MeV/nucleon we have ~214 and ~240 MeV/c per incident nucleon, while ^{6}Li gives a result of ~220 MeV/c. These results again suggest that ^{6}Li is more akin to lighter projectiles than to heavier ones.

D. Comparisons with calculations

1. ISABELLE-EVA

It has been shown [8] that the intranuclear cascade-evaporation simulation ISABELLE-EVA [36,37] provides a reasonable prediction of the LMT and mass yield distribution for the interaction of Cu with 90 MeV/nucleon ^{12}C. We have utilized these same codes to make comparisons with the present 90 MeV/nucleon ^{6}Li + ^{nat}Cu reaction. Using 10 000 cascade-evaporation events, ~6900 for ^{63}Cu and the rest for ^{65}Cu, we have generated the mass-yield and fractional velocity transfer distributions.

In Fig. 8 we compare the mass yield distribution generated by the calculation with the experimental curve. The calculation appears to predict the overall shape of the distribution fairly well although several discrepancies may be noted. Thus for near-target products the calculation overpredicts the cross sections while for the low mass products it underpredicts them. However, the slope of the exponential region of the distribution is adequately reproduced. The underestimation of those products farthest removed from the target may be a consequence of binary fragmentation of the target residue, a process that is not incorporated in the evaporation code. We have also utilized codes that do take binary fragmentation into account (GEMINI, PACE), yet these were also unable to predict the relatively large yields of low mass products. These results will be shown in the following section. The overestimation of the yields of near-target products indicates a problem with the treatment of peripheral interactions, possibly resulting from approximations in the nuclear density distribution in the surface region [36]. Note that the simulation reproduces the sharp decrease in product yields above $A \approx 63$. At least in part, this decrease must be a consequence of the low abundance in a natural copper target of ^{65}Cu which, as already noted, is the primary source of these products.

Figure 9 displays a comparison of the calculated and experimental fractional velocity transfers. The calculation predicts the shape of the distribution well and quantitatively reproduces the values for the $\Delta A = 10$-20 products. Yet for the near-target products the velocity transfers are substantially underestimated. An interesting result of the calculation is the appearance of a plateau in the distribution above $\Delta A \approx 25$, comparable to the experimental plateau, although the uncertainties associated with these low yield products are quite large.

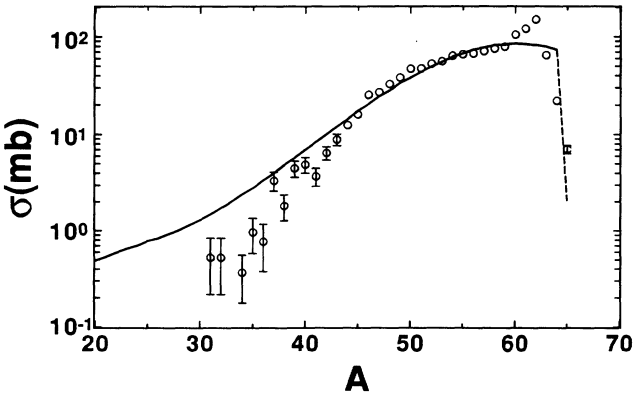

FIG. 8. Comparison of the experimental (curve) and ISABELLE-EVA (○) calculated mass yield distribution for 90 MeV/nucleon ^{6}Li + Cu. The uncertainties in the calculated cross sections reflect the number of events leading to a particular product.

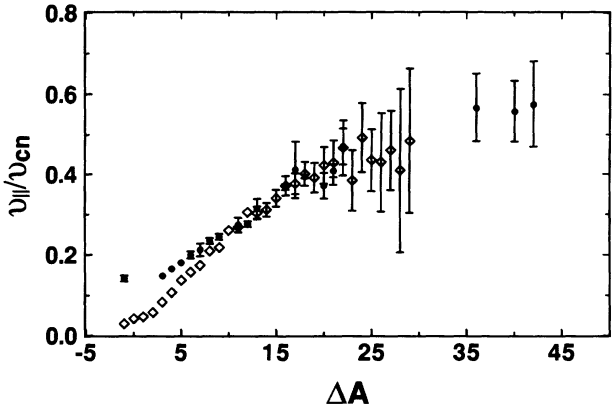

FIG. 9. Comparison of the experimental (•) and ISABELLE-EVA, calculated (◇) fractional velocity transfers.

2. BUU-GEMINI, BUU-PACE

Since mean-field effects are believed to continue to play a role in the reaction dynamics at energies of present interest, we have performed calculations using the Boltzmann-Uehling-Uhlenbeck (BUU) transport equation [38,39], which describes the reaction in terms of mean-field and nucleon-nucleon collisions, to simulate the present reaction. We have coupled this calculation with the deexcitation codes GEMINI [40] and PACE [41] in order to produce observable reaction products along with their kinematic properties.

For each interaction of 90 MeV/nucleon ^{6}Li + ^{64}Cu each nucleon was represented by 100 test particles in BUU. A complete simulation run consisted of 100 individual simulations over a range of impact parameters from $b = 0$ to $b \approx 7$ fm, where the number of simulations per unit impact parameter corresponded to the geometric cross section for that interval. The calculation follows each test particle through six dimensional phase space to a stopping time, t_{stop}, of 60 fm/c, using time steps of 1.5 fm/c. This value of t_{stop} was chosen on the basis of a calculation of the excitation energy of the residual nucleus, E^*, as a function of this parameter. Figure 10 displays this variation for $b = 1.5$, 3.0, and 5.5 fm. The peak in E^* observed at t_{stop} ~30 fm/c reflects the overlap between target and projectile during the early stages of the interaction. However, by t_{stop} ~60 fm/c, a time sufficiently long for the projectile to traverse the target, E^* becomes insensitive to t_{stop} and so our chosen value is appropriate for the system under consideration. We also compared the above results with others obtained for a time step of 1.0 fm/c and found no significant varia-

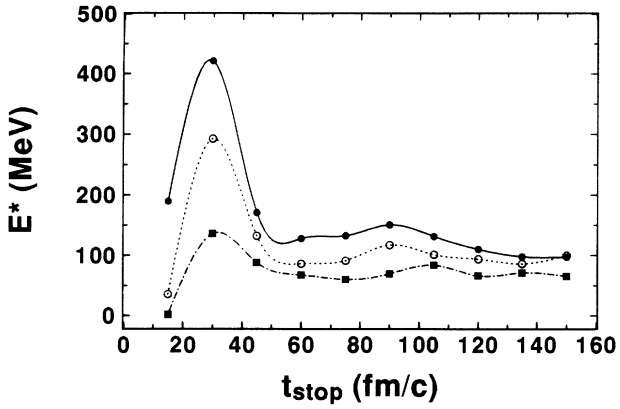

FIG. 10. Dependence of the excitation energy from BUU on t_{stop}. Results are shown for b= 1.5 fm (—), 3.0 fm (••••), and 5.5 fm (– • –).

tion between the two. Calculations were also performed in which each nucleon was represented by 200 test particles. Again, no significant variation in reaction products was found.

A residue was chosen by determining for the target remnant the local nucleon number density in a cubic cell of 1 fm^3 around each nucleon. We then considered those nucleons with a local density of $\rho > 0.021$ fm^{-3} as being bound [42]. We compared these results with a prescription considering particles bound at $\rho > 0.016$ fm^{-3} and found little variation in the reaction products. From these bound nucleons we obtained the Z and A of the residue. The linear momentum of the residue was calculated by

$$P_{\|} = \sum_{i=1}^{A_{res}} p_z(i) \tag{3}$$

and the residue angular momentum by

$$L = \sum_{i=1}^{A_{res}} r_i \times p_i, \tag{4}$$

where the summations were carried out over all test particles in the target residue and then divided by the number of test particles used to represent a single nucleon.

In BUU the Skyrme parametrization is used to estimate the nuclear mean field:

$$U = a(\rho/\rho_0) + b(\rho/\rho_0)^{\sigma}, \tag{5}$$

where ρ_0 is the normal nuclear matter density, taken to be 0.168 fm^{-3}. We have utilized three variations of this parametrization in our comparisons with data, corresponding to an intermediate equation of state (EOS), where $a = -218$ MeV, $b = 164$ MeV, and $\sigma = 4/3$; a soft EOS, where $a = -356$ MeV, $b = 303$ MeV, and $\sigma = 7/6$; and a stiff EOS where $a = -124$ MeV, $b = 70.5$ MeV, and $\sigma = 2$.

The binding energy of the residue was approximated using [42,43]

$$E_{\text{bind}} = -\sum_{i=1}^{A_{res}} \left[p_i^2/2m + (e^2/2) \sum_{j+i} Z(i)Z(j)|r_i - r_j|^{-1} + \frac{1}{2}\, a[\rho(r_i)/\rho_0] + b[\rho(r_i)^{\sigma}/\rho_0^{\sigma}(\sigma + 1)] \right], \tag{6}$$

where a, b, and σ are from the Skyrme parametrization, $e^2 = 1.44$ MeV fm, ρ (r_i) is the local density of an individual particle i and p_i is the relative momentum of the given test particle i. The excitation energy of the residue was then calculated using [42,43]

$$E^* = [8 \text{ MeV/nucleon} - E_{\text{bind}}/\text{nucleon}]A_{\text{res}}. \tag{7}$$

For each individual BUU simulation 100 GEMINI deexcitations were performed, using the Z, A, E^*, $P_{\|}$, and L values from BUU as input. Therefore, for each complete reaction simulation approximately 10^4 reaction products were obtained. The calculated residue cross sections were normalized to the experimental total reaction cross section, 1310 mb.

The mass yield distribution predicted by BUU-GEMINI for the soft and stiff EOS are compared with the experimental curve in Fig. 11(a). The calculation does not fit the data well, although the agreement improves in going from a stiff to soft EOS. For the stiff EOS the peak in the distribution is at a much lower mass than the peak in the experimental mass yield. The calculated yield then falls off very sharply toward lower mass products. The soft EOS predicts a very similar shape for the distribution but is shifted towards larger mass and therefore more closely predicts the peak in the experimental distribution.

We have also examined the effect of changes in the nucleon-nucleon cross section, since the excitation energy has been shown to be sensitive to this quantity [44]. An increase in σ_{NN} improves the agreement for the soft EOS by increasing the yields of the low mass products. However, even for a factor-of-two increase in σ_{NN} the calculation still does not predict the experimental mass yield distribution with any degree of accuracy.

We believe this discrepancy arises from the fact that BUU uses test particles that are grouped into parallel simulations, where the mean field and in turn the residual properties are calculated from an ensemble average. This has the effect of averaging out fluctuations due to nucleon-nucleon collisions [43–45] and leads to unrealistically narrow distributions in E^* and particularly in target residue mass. Thus for each of the various BUU simulations, $A_{\text{res}} \approx 58$–62 and $E^* \approx 5 - 140$ MeV, much narrower than predicted by ISABELLE as shown for the A_{res} distribution in Fig. 12. Note, in addition, that ISABELLE predicts remnants that are some five mass

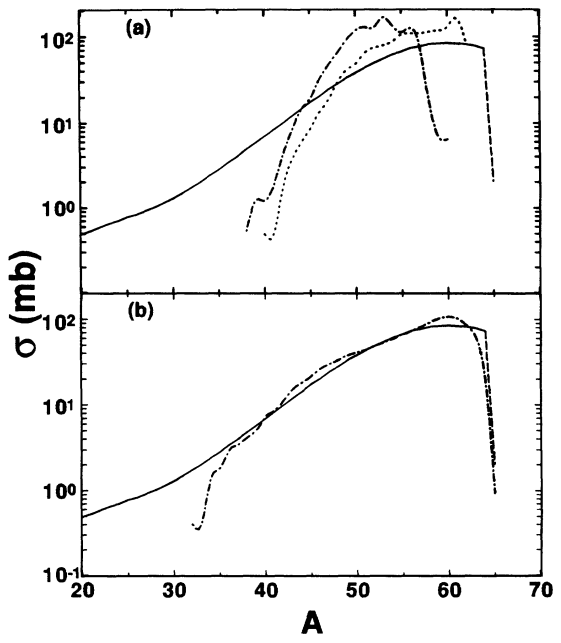

FIG. 11. Comparison of the experimental (—) and (a) ensemble averaged BUU-GEMINI mass yield distribution for a stiff (– • – •) and soft (• • ••) EOS; (b) single parallel BUU-PACE mass yield distribution (–•–) for a soft EOS.

numbers larger than BUU values. The fact that $A_{\rm res} \leq 62$ for BUU necessarily leads to a discrepancy with the experimental curve above this mass number.

One method which might better include these fluctuations is to calculate the mass, charge, and excitation energy of the residue one parallel event at a time. This procedure, which is described elsewhere [45,46], leads to 100 excited target residues for each impact parameter utilized, corresponding to the number of test particles used to represent a nucleon. Since we ran 100 BUU simulations, we obtained a total of 10^4 excited target residues for each complete run, along with their respective $P_{\|}$ and L. These excited residues were then deexcited using the code PACE [41] (which was easier to use than GEMINI when the number of different starting nuclei is large). For each target residue a single PACE deexcitation was performed, again resulting in 10^4 reaction products. Results described above for the ensemble averaged BUU-GEMINI simulations were compared with ensemble averaged BUU-PACE simulations. The deexcitation codes yielded nearly identical mass yield distributions, indicating that differences between the two calculations of present interest could not be attributed to the use of different deexcitation codes.

The mass yield distribution predicted by BUU-PACE using a soft EOS for single parallel events is compared with the experimental yield in Fig. 11(b). The inclusion of fluctuations in BUU produces a very good fit to experimental data. The peak and decrease in the exponential region of the distribution are both very well represented, although the calculation slightly overpredicts near-target products and fails to reproduce the yields of products farthest removed from the target. Also, the decrease in production cross section above $A = 63$ is reproduced. It is interesting to note that the BUU-PACE distribution strongly resembles the ISABELLE-EVA distribution indicating that nucleon-nucleon collisions are most likely the dominant mechanism for this reaction.

Figure 12 includes the mass distribution of BUU generated target residues for single parallel events. Note the broader single parallel event distribution, where $A_{\rm res} \approx 52 - 66$. Similar results were found for the E^* distribution, where E^* varied between 0 and ~350 MeV for single parallel event runs while E^* for the ensemble average runs terminated at ~140 MeV. The broader mass and excitation energy distributions in turn lead to a broader

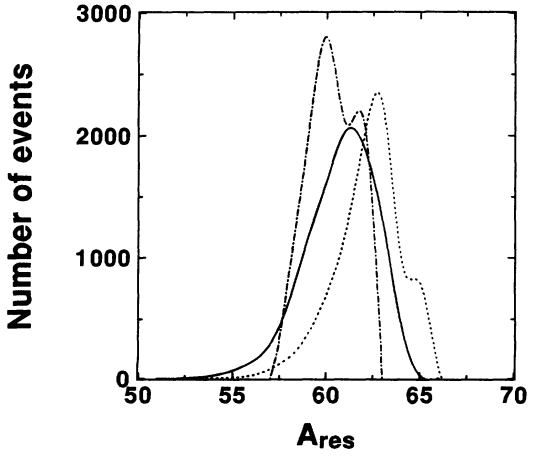

FIG. 12. Mass distribution of excited target residues, $A_{\rm res}$, for ISABELLE (• • ••) and for ensemble averaged (–•–•) and single parallel event (—) BUU calculations.

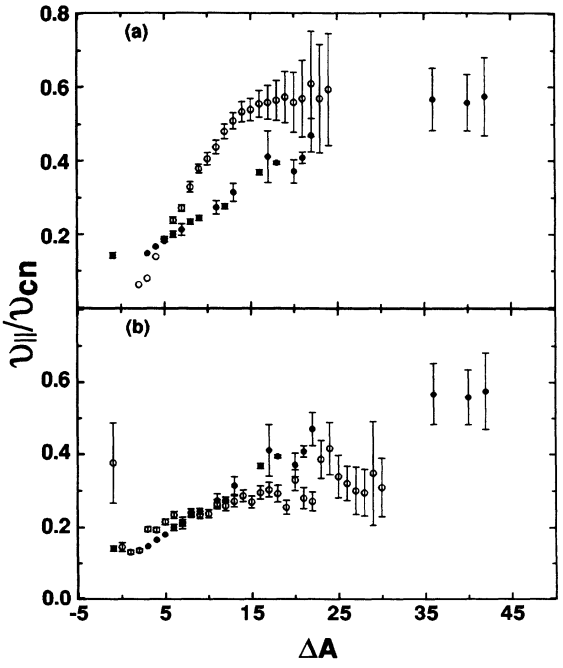

FIG. 13. Comparison of the experimental (•) and BUU (o) fractional velocity transfer for (a) an ensemble average calculation and (b) a single parallel event calculation.

mass yield distribution and thus to better agreement with the data.

The fractional velocity transfer predicted by BUU for the ensemble averaged run and the single parallel event run using a soft EOS are compared with data in Figs. 13(a) and 13(b), respectively. For the ensemble averaged run the calculation fails to reproduce the experimental distribution. The $v_{\|}$ of near target products are severely underestimated, and the increase in $v_{\|}$ with increasing ΔA is much steeper than the experimental trend. The calculation does predict a plateau in $v_{\|}/v_{\mathrm{CN}}$ at $\Delta A \approx 17-25$ and, although the statistical uncertainty of these low yield products is quite large, there does appear to be a limit to the predicted momentum transfer. This limit corresponds to $\sim$200 MeV/c per incident nucleon, in agreement with previously reported experimental results [5,6,8,11,17–21].

In Fig. 13(b), where fluctuations are included, the intermediate and heavy residue fractional velocity transfers are predicted much better, while the light products are somewhat underestimated. Here too, the inclusion of fluctuations leads to much better overall agreement with experiment.

V. CONCLUSION

The interaction of copper with 90 MeV/nucleon ^{6}Li has been investigated and compared with a wide variety of data obtained for lighter and heavier projectiles over a range of energies. The isobaric yield distribution remains essentially unchanged with varying projectile mass and energy up to at least ^{12}C and $\sim$1 GeV total kinetic energy. The ^{6}Li mass yield peaks at approximately $A = 60$ consistent with distributions for lighter projectiles. Heavier ions lead to a peak in the distribution at $3-6$ mass units lower. This difference may be an indication that preequilibrium emission may be more extensive for heavier ions at comparable total kinetic energies. Also, the ^{6}Li mass yield displays no upturn in the distribution at low mass number, while ^{12}C at comparable kinetic energies yields a significant upturn, indicating that heavier ions are more likely to induce fragmentation.

Analysis of LMT data reveals that at comparable energy/nucleon lighter ions are more efficient at transferring their momentum on a per nucleon basis than heavier ions. Also, above the fermi energy the amount of LMT per incident nucleon appears to scale with total projectile kinetic energy for the heavy ions of present interest. In addition, there appears to be a limit in the fractional momentum transfer corresponding to $\sim$220 MeV/c per projectile nucleon. Our results confirm in this respect those of previous work.

Comparisons have been made between experimental results and the intranuclear cascade-evaporation code ISABELLE-EVA. The mass yield distribution is reasonably well reproduced by the calculation, although the predicted yields of near-target and low-mass products differ from the experimental yields. The fractional velocity transfer distribution is also fairly well reproduced, including the appearance of a plateau in the distribution for those products farthest removed from the target, but the velocities of near-target products are underestimated.

Comparisons have also been made with BUU-GEMINI and BUU-PACE simulations. Various equations of state and nucleon-nucleon cross section values have been used in the interaction calculation. For ensemble averaged runs, neither the mass yield distribution nor the fractional velocity transfer distribution is well reproduced by the calculation, presumably due to exclusion of fluctuations in the calculation. On the other hand, the use of single parallel events from BUU, which roughly preserve the fluctuations, reproduces the mass yield distribution quite well. Also, the fractional velocity distribution is adequately reproduced.

ACKNOWLEDGMENTS

We wish to thank R. Ronningen and the members of the NSCL for their assistance and cooperation. We also wish to thank W. Bauer for the BUU code and insightful conversations concerning its operation, and R. Charity for the GEMINI code. This work was supported by the U.S. Department of Energy.

[1] E. Hagebø, I. R. Haldorsen, M. B. Mostue, J. Pettersen, Ø. Scheidmann, T. Lund, L. C. Carraz, and C. Richard-Serre, Radiochim. Acta **35**, 133 (1984).
[2] C. J. Orth, H. A. O'Brien, Jr., M. E. Schilliac, B. J. Dropesky, J. E. Cline, E. B. Nieschmidt, and R. L. Brodzinski, J. Inorg. Nucl. Chem. **38**, 13 (1976).
[3] P. J. Karol, Phys. Rev. C **10**, 150 (1974).
[4] E. Gadioli, E. Gadioli Erba, D. J. Parker, and J. Asher, Phys. Rev. C **32**, 1214 (1985).
[5] J. Jastrebski, P. P. Singh, T. Moróz, H. J. Karwowski, S. E. Vigdor, and M. Fatyga, Phys. Lett. **136B**, 169 (1984).
[6] J. Jastrebski, P. P. Singh, T. Moróz, S. E. Vigdor, M. Fatyga, and H. J. Karwowski, Phys. Rev. C **34**, 60 (1986).
[7] W. Skulski, J. Jastrebki, P. P. Singh, Q. Chen, and M. Fatyga, Phys. Rev. C **41**, 2605 (1990).
[8] J. P. Whitfield and N. T. Porile, Phys. Rev. C **47**, 1636 (1993).
[9] S. Y. Cho, Y. H. Chung, N. T. Porile, and D. J. Morrissey, Phys. Rev C **36**, 2349 (1987).
[10] S. Y. Cho, N. T. Porile, and D. J. Morrissey, Phys. Rev. C **39**, 2227 (1989).
[11] L. Pieńkowski, J. Jastrebski, W. Kurcewicz, A. Gizon, J. Blachot, and J. Crancon, Phys. Rev. C **43**, 1331 (1991).
[12] T. Lund, D. Molzahn, R. Brandt, B. Bergersen, D. Eriksen, E. Hagebø, I. R. Haldorsen, T. Bjørnstad, and C. Richard-Serre, Phys. Lett. **102B**, 239 (1981).
[13] T. Lund, D. Molzahn, B. Bergersen, E. Hagebø, I. R. Haldorsen, and C. Richard-Serre, Z. Phys. **A306**, 43 (1982).
[14] A. Lleres, J. Blachot, J. Crancon, A. Gizon, and H. Nifenecker, Z. Phys. **A312**, 177 (1983).

[15] L. Kowalski, P. E. Haustein, and J. B. Cumming, Phys. Rev. Lett. **51**, 642 (1983).
[16] K. Krishan, S. Bhattacharya, J. N. De, and S. K. Samaddar, Nucl. Phys. **A495**, 65c (1989).
[17] J. Galin *et al.*, Phys. Rev. Lett. **48**, 1787 (1982).
[18] G. Nebbia *et al.*, Z. Phys. **A311**, 247 (1983).
[19] J. L. Laville *et al.*, Phys. Lett. **138B**, 35 (1984).
[20] V. E. Viola, Nucl. Phys. **A471**, 55c (1987).
[21] M. B. Tsang *et al.*, Phys. Lett. **134B**, 169 (1984).
[22] F. Saint-Laurent *et al.*, Phys. Lett. B **202**, 190 (1988).
[23] G. LaRana *et al.*, Nucl. Phys. **A407**, 233 (1983).
[24] S. Leray, J. Phys. **C4**, 275 (1986).
[25] T. Batsch *et al.*, Phys. Lett. B **189**, 287 (1987).
[26] F. Hubert, A. Fleury, R. Bimbot, and D. Gardes, Ann. Phys. (Paris) **5**, 1 (1980).
[27] J. F. Ziegler, J. P. Biersack, and U. Littmark, in *The Stopping and Ranges of Ions in Matter* (Pergamon, New York, 1985), Vol. 1.
[28] T. Routti and S. G. Prussin, Nucl. Instrum. Methods **72**, 125 (1969).
[29] J. B. Cumming, National Academy of Sciences Report No. NAS-NS-3107, 1962 (unpublished), p. 25.
[30] U. Reus and W. Westmeier, At. Data Nucl. Data Tables **29**, 2 (1983).
[31] Y. H. Chung, S. Y. Cho, and N. T. Porile, Nucl. Phys. **A533**, 170 (1991).
[32] G. Rudstam, Z. Naturforsch. **219**, 1027 (1966).
[33] J. B. Cumming, P. E. Haustein, T. J. Ruth, and G. J. Virtes, Phys. Rev. C **17**, 1632 (1978).
[34] J. P. Whitfield and N. T. Porile, Nucl. Phys. **A550**, 553 (1992).
[35] M. Fatyga, K. Kwiatkowski, V. E. Viola, C. B. Chitwood, J. D. Fields, C. K. Gelbke, W. G. Lynch, J. Pochadzalla, M. B. Tsang, and M. Blann, Phys. Rev. Lett. **55**, 1376 (1985).
[36] Y. Yariv and Z. Fraenkel, Phys. Rev. C **20**, 2227 (1979); *ibid.* **24**, 488 (1981).
[37] I. Dostrovsky, Z. Fraenkel, and G. Friedlander, Phys. Rev. **116**, 683 (1959).
[38] W. Bauer, G. F. Bertsch, W. Cassing, and U. Mosel, Phys. Rev. C **34**, 2127 (1986).
[39] W. Bauer, Phys. Rev. Lett. **61**, 2534 (1988).
[40] R. J. Charity *et al.*, Nucl. Phys. **A483**, 371 (1988).
[41] A. Gavron, Phys. Rev. C **21**, 230 (1980).
[42] D. R. Bowman *et al.*, Phys. Rev. C **46**, 1834 (1992).
[43] W. Bauer, private communication.
[44] H. M. Xu, P. Danielewicz, and W. G. Lynch, Phys. Lett. B **299**, 199 (1993).
[45] W. Bauer, G. F. Bertsch, and S. Das Gupta, Phys. Rev. Lett. **58**, 863 (1987).
[46] G. F. Bertsch and S. Das Gupta, Phys. Rep. **160**, 189 (1988).